B. E. Launder
Department of Mechanical Engineering,
University of California,
Davis, Calif. 95616

M. A. Leschziner
Sonderforschungsbereich 80,
University of Karlsruhe,
Karlsruhe, West Germany

Flow in Finite-Width Thrust Bearings Including Inertial Effects

II—Turbulent Flow

A new set of turbulent resistance laws for hydrodynamic lubricant films has been derived with the aid of a turbulence model which includes transport effects on two turbulence parameters. The model consists of two differential equations for the turbulence energy and its rate of dissipation and a constitutive equation for the turbulent viscosity. The model places no restrictions on the Reynolds number.

An efficient finite-difference scheme, based on the integro-differential approach and incorporating the resistance laws and a set of accurate inertial coefficients, is applied to the solution of the turbulent inertial flow in finite-width slider bearings. A selection of predictions is presented for non-inertial and inertial flows. The former are compared with solutions obtained with alternative turbulent lubrication theories. The importance of including fluid inertia effects is demonstrated.

1 Introduction

Recent years have seen a steady increase in operating speeds and in the use of unconventional, low kinematic-viscosity fluids in lubrication applications. One outcome of this trend is that the flow in lubricating films is, in an increasing number of cases, turbulent. The tribologist thus needs to pay closer attention to the formulation of accurate resistance laws for turbulent transport over a widening range of conditions. Although the practice-oriented engineer is ultimately concerned only with operational characteristics, such as frictional losses and load-carrying capacity, these are, in fact, governed by the details of the turbulent transport processes in the lubricant film itself. Thus, in order to devise a widely applicable set of flow resistance laws, a turbulence theory—or "model"—is required of turbulent transport processes.

In many fluid-flow related fields other than tribology, mathematical modeling of turbulence has, for many years, been the subject of intensive research. As a result, a large number of models of varying degrees of complexity and generality have emerged [1]. The general trend has been towards the use of more complex and widely applicable transport models, which concern themselves increasingly with the details of the flow. Advances in turbulent lubrication theory have, however, not followed the same pattern as in other branches of fluid mechanics. The mixing-length treatments of Constantinescu [2, 3], Arwas, et al. [4] and others have been followed by analyses such as those of Reynolds [6], Ng and Pan [7], Elrod and Ng [8], and Hirs [9] where more rudimentary global-resistance treatments were adopted. (An extensive review of most theoretical approaches to turbulent lubrication is provided in [10].)

Recently, however, this pattern has been reversed with the work of Ho and Vohr [5] on the use of a 1-equation transport model of turbulence. In this scheme the local turbulent velocity scale in the bearing film is obtained from solving a transport equation for the turbulence kinetic energy. The use of such a model represents a major conceptual advance over previous practices in analyzing turbulent lubricant films. It is unfortunately the case, however, that in other fields of fluid mechanics [1] models of this kind have not brought the improvement in predictive accuracy that their proponents had expected. To achieve significant improvement in generality over that obtainable with the mixing-length hypothesis one needs to solve at least two turbulence transport equations, effectively for the characteristic length and time-scales of turbulence.

Although there are numerous two-equation turbulence models in the literature, very few are suitable for application to flow in lubricant films. This class of flows is usually characterized by relatively low Reynolds numbers and by steep pressure gradients. These circumstances mean that significant variations in fluid shear stress occur over the region near the wall where molecular transport is important—a region which is intrinsically treated as a uniform stress layer in most available two-equation models.

Reference [11] has presented a model not subject to these limitations and, indeed, has applied it successfully to predict the partial reversion of turbulent to laminar flow due to steep streamwise accelerations. Other successful applications of the model include low

Contributed by the Lubrication Division for publication in the JOURNAL OF LUBRICATION TECHNOLOGY. Manuscript received at ASME Headquarters, May 1, 1978.

 Copyright © 1978 by ASME

Downloaded 16 Aug 2012 to 165.91.101.108. Redistribution subject to ASME license or copyright; see http://www.asme.org/terms/Terms_Use.cfm

Reynolds number flow in pipes and channels [12] and swirling flow near walls [13], the latter bearing fairly close relation to non-planar flows in bearing films. Accordingly we have employed this model as the basis of the present work within the framework of an integro-differential approach [14, 15]. The transport model is used to generate a new set of turbulence resistance laws and inertial coefficients for hydrodynamic bearing films. These laws and coefficients are then used in conjunction with an efficient numerical scheme [16] to simulate the turbulent inertial flow in plane sliders.

2 General Principles of the Mathematical Formulation

The flow within a lubricant film, as sketched in Fig. 1, is strictly governed by the three-dimensional form of the momentum and continuity equations. To undertake a three-dimensional numerical treatment, however, would be prohibitively expensive, particularly if a multi-equation turbulence transport model were to be used. Fortunately, the very small thickness of the film compared with its other dimensions allows considerable simplification. Following Slezkin and Targ [14], Constantinescu [15] and others, we show in [16] that the dynamics of the flow in plane lubricant films may be represented by the following set of two-dimensional integro-differential equations.

$$\int_0^h \rho\left(\frac{\partial u^2}{\partial x}+\frac{\partial uv}{\partial y}\right)dz = -h\frac{\partial p}{\partial x}+(\tau_{xz,h}-\tau_{xz,0}) \tag{2.1}$$

$$\int_0^h \rho\left(\frac{\partial uv}{\partial x}+\frac{\partial v^2}{\partial y}\right)dz = -h\frac{\partial p}{\partial y}+(\tau_{yz,h}-\tau_{hz,0}) \tag{2.2}$$

$$\frac{\partial(\rho h u_m)}{\partial x}+\frac{\partial(\rho h v_m)}{\partial y}=0 \tag{2.3}$$

To obtain solutions to the above set, the unknown shear-stress and inertial terms need to be expressed as functions of the determinable mass-mean velocities u_m and v_m. To this end, it is assumed that, as in the case of laminar flows, inertia influences the magnitude of the mass-mean velocities but not the shape of the velocity profiles. In laminar flow simple analytic expressions are available for the non-inertial velocity distributions across the film which may readily be used to derive frictional and inertial contributions to the momentum balance in terms of mean velocities. Such analytic results cannot be obtained for turbulent flow, however, due to the highly complex variation of effective viscosity across the film.

Instead, the relation between friction components and mean velocities is obtained by solving numerically the noninertial equations of motion across the film.

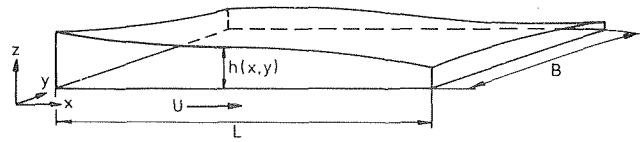

Fig. 1 The film topography

$$\frac{\partial}{\partial z}(\mu+\mu_t)\frac{\partial u}{\partial z}=\frac{\partial p}{\partial x} \tag{2.4}$$

$$\frac{\partial}{\partial z}(\mu+\mu_t)\frac{\partial v}{\partial z}=\frac{\partial p}{\partial y} \tag{2.5}$$

wherein the turbulent viscosity, μ_t, is obtained from the chosen turbulence model. As discussed in Section 1, the present work adopts a two-equation model because of the evidence that it will be more widely applicable than simpler alternatives to the kinds of flow arising in lubricant passages. Knowledge of the velocity profiles then enables the mean velocities, the wall shear stresses and the inertial terms to be obtained. The task appears straightforward. However, because of the cross-coupling between the turbulent viscosity and the velocities, a large number of computations are required to generate correlations linking the shear stresses and inertial terms to suitable flow parameters. The precise form of the correlations and the way in which they have been generated is considered in detail in Section 4. It is here appropriate however, to outline briefly how the present treatment differs from those previously adopted.

Several workers (e.g., [3, 5, 7–8]) expressed frictional effects by way of the following parameters.

$$k_x \equiv \frac{(\tau_{xz,h}-\tau_{xz,0})h}{\mu\left(\frac{U}{2}-u_m\right)} \tag{2.6}$$

$$k_y \equiv \frac{(\tau_{yz,h}-\tau_{yz,0})h}{-\mu v_m} \tag{2.7}$$

Only references [5] and [8] took full account of the cross-coupling between turbulent viscosity and velocities by relating k_x and k_y to the pressure gradients as well as to the sliding Reynolds number.

$$k_x = k_x(\mathrm{Re}, \nabla p^*)$$

$$k_y = k_y(\mathrm{Re}, \nabla p^*) \tag{2.8}$$

Nomenclature

B = width of bearing pad
c_μ, c_1, c_2, c_3 = turbulence model constants
c_f = friction factor [$= 2\tau_w/\rho u_m^2$]
$c_{sxE}, c_{syE}, c_{sxI}, c_{syI}$ = wall shear stress coefficients (equations (5.6) to (5.9))
$\overline{F}_s$ = nondimensional shear force on sliding plate [$= F_s h_2/\mu ULB$]
h = film thickness
h_1 = film thickness at leading edge of bearing pad
h_2 = film thickness at trailing edge of bearing pad
k = turbulence energy
k_x, k_y = flow rate coefficients (equations (5.7), (5.2))
L = length of bearing pad
p = static pressure
$\overline{p}$ = nondimensional static pressure [$\overline{p} = ph_2^2/\mu UL$]
$\overline{p}_b$ = nondimensional mean pressure over bearing pad
$\overline{q}_i, \overline{q}_0$ = nondimensional flow rate through leading and trailing edge of bearing pad [$\overline{q}_i = 2q_i/Uh_2B; \overline{q}_0 = 2q_0/Uh_2B$]
Re = sliding Reynolds number [$= \rho Uh/\mu$]
Re* = film Reynolds number [$Uh_2/\nu \cdot h_2/L$]
Re_m = mean sliding Reynolds number [$= U\overline{h}/\nu$]
Re_p = Reynolds number for channel flows [$= 2u_m h/\nu$]
U = sliding velocity
u = velocity in x-direction
u_m = mass-mean velocity across film in x-direction
$\overline{u}_m$ = nondimensional mass-mean velocity [$\equiv u_m/U$]
u_t = nondimensional velocity in x-direction [$= u/\sqrt{\tau_w/\rho}$
v = velocity in y-direction
v_m = mass-mean velocity
$\overline{v}_m$ = nondimensional mass-mean velocity [$\equiv v_m/U$]
x, y, z = Cartesian coordinates
z_1 = nondimensional distance from a wall [$= z\sqrt{\tau_w\rho/\mu}$]
$\delta_{xx}, \delta_{xy}, \delta_{yy}$ = inertial coefficients (equations (5.3) to (5.5))
ϵ = rate of turbulence energy dissipation
μ = fluid viscosity
μ_t = turbulent viscosity
ν = kinematic fluid viscosity
ρ = fluid density
$\sigma_\kappa, \sigma_\epsilon$ = Prandtl numbers for turbulence energy and dissipation
σ = standard deviation
τ_w = wall shear stress
$\tau_{xz,0}, \tau_{xz,h}$ = wall shear stresses in x-direction on sliding and stationary surfaces
$\tau_{yz,0}, \tau_{yz,h}$ = wall shear stresses in y-direction on sliding and stationary surfaces
τ_t = nondimensional shear stress [$= \tau/\tau_w$]
ϕ = any frictional or inertial coefficient

Downloaded 16 Aug 2012 to 165.91.101.108. Redistribution subject to ASME license or copyright; see http://www.asme.org/terms/Terms_Use.cfm

where

$$\nabla p^* = \left[\left(\frac{\partial p}{\partial x}\right)^2 + \left(\frac{\partial p}{\partial y}\right)^2\right]^{1/2} \frac{h^3}{\mu\nu}$$

In the present study, k_x and k_y have been expressed as functions of the nondimensional mass-mean velocities rather than the pressure gradients. This difference is by no means merely cosmetic for, in the presence of inertia, the wall-shear stresses are no longer uniquely related to the pressure gradients, but they *are* uniquely related to the mean velocities—provided, of course, the shape of the profiles is assumed invariant with inertia. Moreover, in contrast to previous work, the present study provides accurate correlations for all the inertia terms appearing in equations (2.1) and (2.2).

3 The Turbulence Model

The present work has adopted the low-Reynolds number energy-dissipation model of turbulence [11]. In this model, the turbulent viscosity is given by:

$$\mu_t = c_\mu \rho k^2/\epsilon \tag{3.1}$$

where the turbulence energy k and its dissipation rate ϵ are determined from differential transport equations. Exact equations for k and ϵ may be derived from the Navier-Stokes equations, but the resultant equations contain unknown correlations between fluctuating quantities that need to be approximated or "modeled" to produce a closed set. The derivation of the exact equations is presented, for example, by Daly and Harlow [17] while the closure is discussed in detail in references [12] and [18]. Here therefore only the final forms of the k and ϵ equations, applicable to inertia-less, nonplanar flows in thin films, are given:

$$\frac{d}{dz}\left[\left(\mu + \frac{\mu_t}{\sigma_k}\right)\frac{dk}{dz}\right] + \mu_t\left[\left(\frac{du}{dz}\right)^2 + \left(\frac{dv}{dz}\right)^2\right] - \rho\epsilon - 2\mu\left(\frac{dk^{1/2}}{dz}\right)^2 = 0 \tag{3.2}$$

$$\frac{d}{dz}\left[\left(\mu + \frac{\mu_t}{\sigma_\epsilon}\right)\frac{d\epsilon}{dz}\right] + c_1\frac{\epsilon}{k}\mu_t\left[\left(\frac{du}{dz}\right)^2 + \left(\frac{dv}{dz}\right)^2\right] - c_2\rho\frac{\epsilon^2}{k} + c_3\frac{\mu\mu_t}{\rho}\left\{\left[\left(\frac{du}{dz}\right)^2 + \left(\frac{dv}{dz}\right)^{1/2}\right]\right\}^2 = 0 \tag{3.3}$$

In the above, the "turbulent Prandtl numbers" σ_k and σ_ϵ and the coefficients c_μ, c_1, c_2, and c_3 are assigned as follows:

$$c_1 = 1.44;\ c_3 = 2.0;\ \sigma_k = 1.0;\ \sigma_\epsilon = 1.3$$

$$c_2 = 1.92\,[1. - 0.3\exp(-R_t{}^2)]$$

$$c_\mu = 0.09\exp[-3.4/(1 + R_t/50)^2]$$

$$R_t = \rho k^2/\mu\epsilon$$

The above relationships and values are those used in reference [13] to predict swirling flows near spinning disks and cones. They represent reoptimized versions of those originally proposed in references [12] and [18] though, for practical purposes, the original parameters would give essentially the same results.

4 Couette-Flow Characteristics

4.1 The Solving Scheme. The geometry is that of two parallel impervious plates—one of which is sliding—confining a fully established flow. The flow is driven by the x-wise sliding motion and pressure gradients in the x and y directions.

Simultaneous solutions are required of equations (2.4) and (2.5) together with (3.2) and (3.3). The transport equations possess the common form:

$$\frac{d}{dz}\left[\left(\mu + \frac{\mu_t}{\sigma_\phi}\right)\frac{d\phi}{dz}\right] = S_1{}^\phi + S_2{}^\phi\phi \tag{4.1}$$

where $S_1{}^\phi + S_2{}^\phi\phi$ denote the source and sink terms for the quantity ϕ (which may stand for u_m, v_m, k, or ϵ). The set of coupled nonlinear ordinary differential equations has been solved by a finite-difference scheme, details of which are provided in reference [10]. In summary discretized versions of (4.1) are solved with 100–150 nodes distributed non-uniformly along a single line extending between the upper and lower plates. Flow conditions are fixed by prescribing the mass-mean velocities u_m and v_m and the sliding velocity U. Solution of (4.1) then provides profiles of all the ϕ's, the pressure gradients and the wall-shear stresses.

4.2 Predicted Characteristics. Experimental data with which to assess the performance of the turbulence model seem to be available only for the two limiting cases: the purely pressure-driven flow between stationary plates (channel flow) and Couette flow in the absence of streamwise pressure gradients. Predictions of the former flow have been reported in reference [12]. The behavior predicted with the present set of reoptimized coefficients is not significantly different from the original and is therefore not reproduced here. We may remark, however, that accurate predictions are obtained of the friction factor data of Beavers, et al. [19] even at the low-Reynolds-number end of their measurements. This is in contrast with predictions obtained with most other turbulence models which display a progressively too high friction factor as the Reynolds number is reduced below about 10^4.

Predictions obtained for pure Couette flow are presented in Figs. 2–4. Experimental data for this flow are not extensive and, in view of the obvious experimental problems, those that are available should be looked upon with some caution.

Excellent agreement is displayed in Figs. 2 and 3 between the measured velocity profiles of Reichardt [20] and Robertson [21] and the predictions. The Reynolds numbers in the two cases differ by a factor of 13, so the agreement is especially reassuring. We find, how-

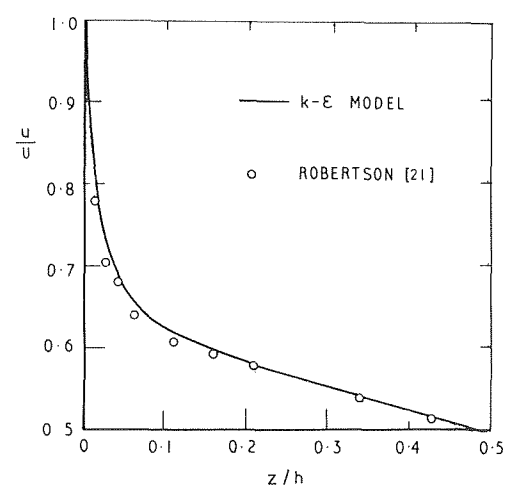

Fig. 2 Velocity profile in pure Couette flow

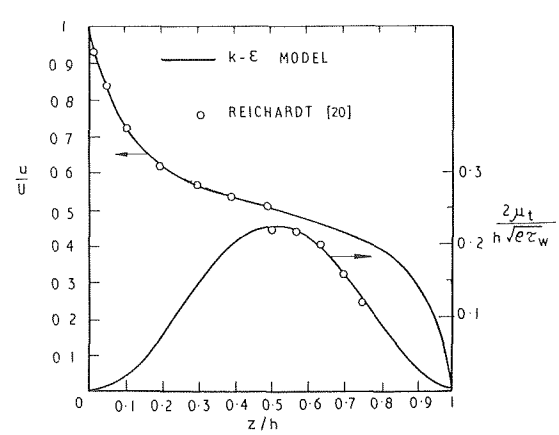

Fig. 3 Velocity and turbulent viscosity profile in pure Couette flow

Downloaded 16 Aug 2012 to 165.91.101.108. Redistribution subject to ASME license or copyright; see http://www.asme.org/terms/Terms_Use.cfm

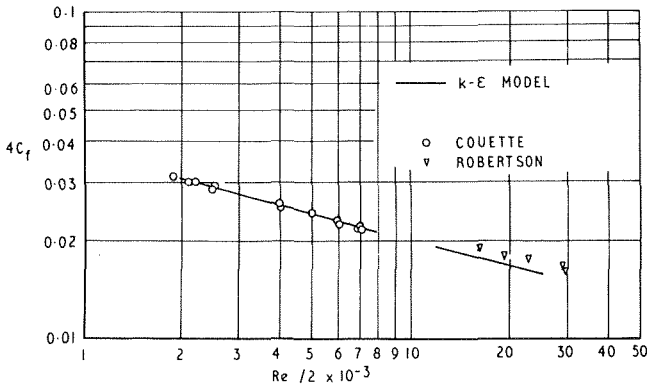

Fig. 4 Friction factors in pure Couette flow

ever, that while the calculated friction factors shown in Fig. 4 are in complete agreement with Couette's [22] original measurements, Robertson's data lie approximately 10 percent above the theoretical values. We note that any subsidiary frictional losses in the system will tend to produce too high measured values.

Here it is appropriate to add that reference [12] has reported the successful application of the present model to flow between converging planes while reference [13] contains equally satisfactory predictions for the case of flow along an annular passage in which the core tube is rotating. It seems reasonable to conclude therefore that the characterization of turbulent transport by the model of Section 3 provides a satisfactory physical basis for problems of turbulent lubrication.

We now examine briefly some of the implications of the model when applied to tribological flows. Selected predictions for velocity profiles, turbulence energy profiles and for the flow-rate parameters k_x and k_y are compared in Figs. 5 to 7 with those of Ho and Vohr [5] obtained with what was, hitherto the most comprehensive turbulence model used in turbulent lubrication. Figs. 5 and 6 show that, for both planar and nonplanar flows, the present model generates higher mass-mean velocities for given values of sliding velocity and pressure gradients. The k-ϵ model thus predicts lower turbulent viscosities—especially at low Reynolds number. Consistent with this behavior are lower values of k_x and k_y, as shown in Fig. 7.

5 The Resistance Laws and Inertial Coefficients

Following the general principles outlined in Section 2 the following nine coefficients have been evaluated as functions of R_e, u_m/U, and v_m/U with the aid of the k-ϵ model:

$$k_x \equiv \frac{h(\tau_{xz,h} - \tau_{xz,0})}{\mu\left[\frac{U}{2} - u_m\right]} \tag{5.1}$$

$$k_y \equiv \frac{h(\tau_{yz,h} - \tau_{yz,0})}{\mu v_m} \tag{5.2}$$

$$\delta_{xx} \equiv \frac{\int_0^h \rho u^2\, dz}{\rho h u_m{}^2} \tag{5.3}$$

$$\delta_{xy} \equiv \frac{\int_0^h \rho u v\, dz}{\rho h u_m v_m} \tag{5.4}$$

$$\delta_{yy} \equiv \frac{\int_0^h \rho v^2\, dz}{\rho h v_m{}^2} \tag{5.5}$$

$$c_{sxI} \equiv \frac{\tau_{xz,0} \cdot h}{\mu u_m} \tag{5.6}$$

$$c_{syI} \equiv \frac{\tau_{yz,0} \cdot h}{\mu v_m} \tag{5.7}$$

$$c_{sxE} \equiv \frac{\tau_{xz,h} \cdot h}{\mu u_m} \tag{5.8}$$[1]

$$c_{syE} \equiv \frac{\tau_{yz,h} \cdot h}{\mu v_m} \tag{5.9}$$[1]

With coefficients (5.1) to (5.5), equations (2.1) and (2.2) may be written:

$$\frac{\partial}{\partial x}(\delta_{xx}\rho u_m{}^2) + \frac{\partial}{\partial y}(\delta_{xy}\rho u_m v_m) = -h\frac{\partial p}{\partial x} + \frac{k_x \mu}{h}\left[\frac{U}{2} - u_m\right] \tag{5.10}$$

$$\frac{\partial}{\partial x}(\delta_{xy}\rho u_m v_m) + \frac{\partial}{\partial y}(\delta_{yy}\rho v_m{}^2) = -h\frac{\partial p}{\partial y} - \frac{k_y \mu}{h} v_m \tag{5.11}$$

Equations (5.10), (5.11), and (2.3) thus form a closed set to be solved for u_m, v_m, and p. Coefficients (5.6) and (5.7) allow, in conjunction with (5.1) and (5.2), the individual wall-shear stresses to be determined.

Due to the complexity of the equation set (4.1) it is not possible to obtain exact analytical relations expressing the dependence of these coefficients on the Reynolds number and the normalized velocities $\bar{u}_m$ and $\bar{v}_m$. Accordingly numerical solutions to (4.1) had to be obtained over a wide range of conditions and the results correlated. We summarize the procedures followed. Results were obtained for 13 values of Reynolds number, the maximum and minimum values being 650 and 40,000, respectively. The values were chosen so that they formed a geometric series with a multiplication factor of approxi-

[1] Strictly, only seven coefficients are needed. If, for instance, k_x and k_y are given, either c_{sxI} and c_{syI} or c_{sxE} and c_{syE} would suffice for the determination of all wall-shear-stress components.

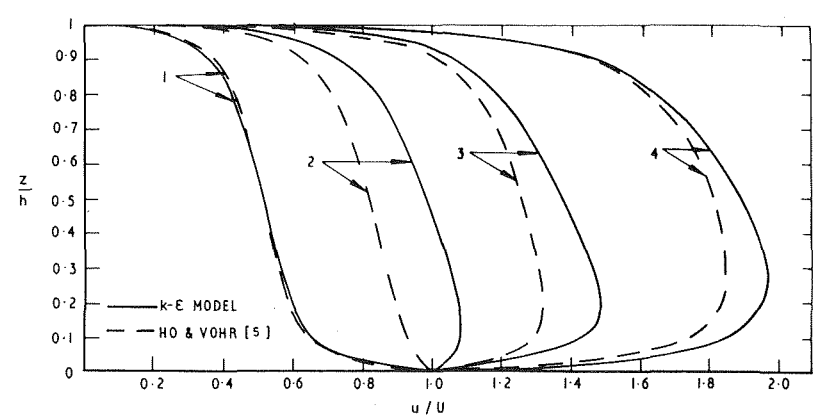

Fig. 5 Predicted velocity profiles in slider direction for 4 levels of pressure gradient

Downloaded 16 Aug 2012 to 165.91.101.108. Redistribution subject to ASME license or copyright; see http://www.asme.org/terms/Terms_Use.cfm

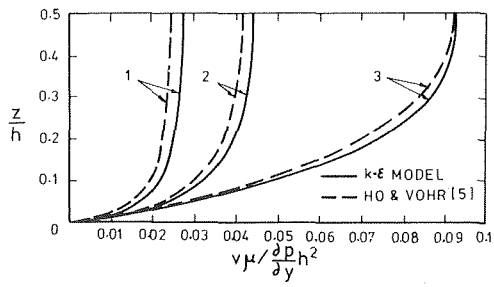

Fig. 6 Velocity profiles normal to sliding direction

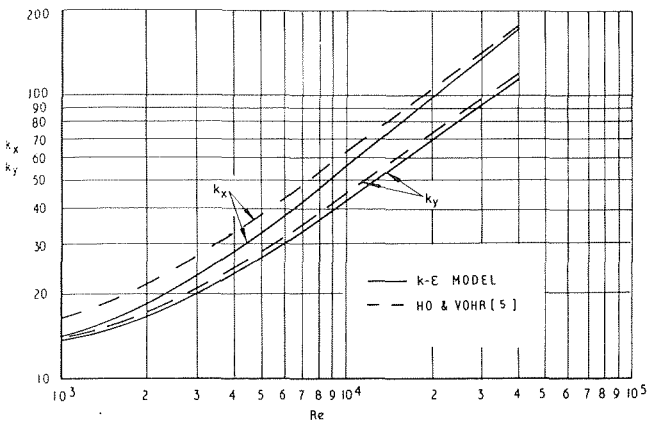

Fig. 7 Variation of predicted resistance coefficients with Reynolds number

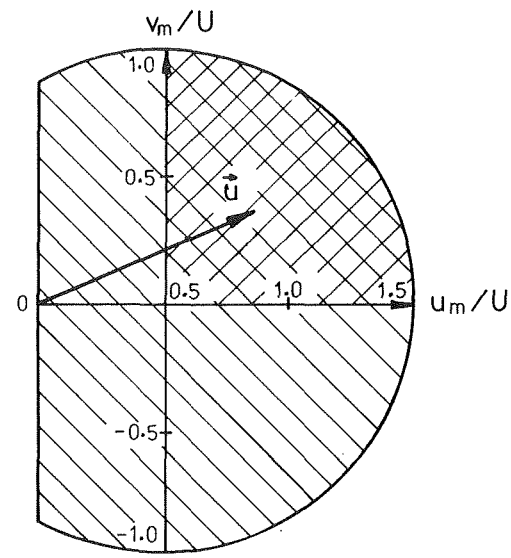

Fig. 8 Hodograph plot showing domain of $\bar{u}_m$ and $\bar{v}_m$ over which resistance coefficients are evaluated

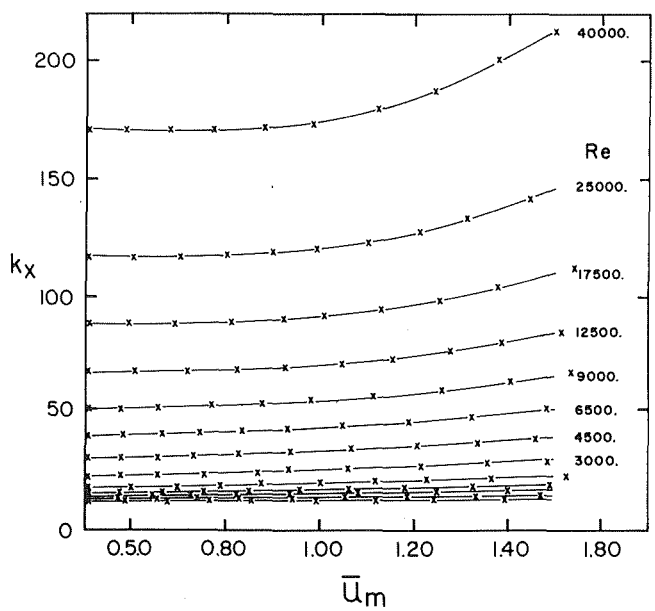

Fig. 9 Comparison of numerical solutions to resistance functions with analytical fit (equation 5.12)

mately 1.4. For each value of Re, the coefficients were computed for approximately 50 combinations of $\bar{u}_m$ and $\bar{v}_m$ within the shaded part of the domain $D'\{\bar{u}_m, \bar{v}_m\}$, shown in Fig. 8, bounded by the line $u_m/U = 0$ and the unit circle centered at $u_m/U = 0.5$, $v_m/U = 0$.

With the exception of δ_{yy}, the coefficients for a given value of v_m were then correlated as functions of Re and $\bar{u}_m$ by a least squares fit to the coefficients of the following polynomial

$$\phi = A_1 + A_2\bar{u}_m + A_3 \log \mathrm{Re} + A_4\bar{u}_m{}^2 + A_5\bar{u}_m \log \mathrm{Re} + A_6 \log \mathrm{Re}^2 + A_{\frac{1}{2}n(n+1)+1}\bar{u}_m{}^n + \ldots A_{\frac{1}{2}(n+1)(n+2)} (\log \mathrm{Re})^n \quad (5.12)$$

where ϕ denotes any of the coefficients to be correlated. δ_{yy} was correlated to Re only as it was found to be almost independent of $\bar{u}_m$ and $\bar{v}_m$. The polynomial degree, n, varied between 3 and 6. In all cases, the relative standard deviation

$$\bar{\sigma} \equiv \frac{\sum_i [(\phi_i - \phi)^2]^{1/2}}{\sum_i [(\phi_i - \phi)]^{1/2}}$$

was found to be less than 10^{-3}. The fitting quality can best be judged from Fig. 9 showing the variation of k_x with $\bar{u}_m$ and Re. Crosses represent values computed while the curves represent sections through the fitted surfaces. A complete set of such figures, together with tables listing the polynomial coefficients is provided in reference [10].†

6.1 Application to Slider Bearings

Numerical solutions for the turbulent inertial flow in finite-width slider bearings were obtained by inserting the analytic correlations (5.12) for coefficients (5.1) to (5.7) into the two-dimensional iterative numerical scheme for laminar flows developed in [16] (in place of the analytical laminar-flow versions of these parameters).

† Copies of the tables of coefficients may be obtained on request from either author. A copy is also deposited with the Engineering Societies Library 345 E. 47th St., New York, N. Y. 10017.

The performance of the resulting scheme is demonstrated in Figs. 10 to 15. These represent a selection of results taken from a parametric study for rectangular pads [10]. The present predictions are compared with non-inertial solutions of Taylor and Dowson [23] obtained with the theories of Constantinescu [3], Ng and Pan [7], and Hirs [9].

First, Figs. 10 to 12 show the effect of the mean Reynolds number Re_m on the pressure field, load capacity and flow rates in a square pad for a contraction ratio $h_1/h_2 = 2$. The ratio h_2/L is 0.002 throughout. Thus, in the presence of inertia, the film Reynolds number Re* rises at the same rate as Re_m, reaching values of 8/3 and 40/3 at $\mathrm{Re}_m = 2000$ and 10,000 respectively. The effect of Re_m is seen to raise the level of pressure while the shape of the pressure distribution remains virtually unaltered. The increase in pressure is primarily a result of the increased frictional resistance rather than of inertial effects—a fact well brought out in Fig. 11(*a*). In contrast, the influence of inertia on the flow rates is more marked as may be seen from Fig. 12.

For noninertial flow, comparison with Taylor and Dowson's solution

Downloaded 16 Aug 2012 to 165.91.101.108. Redistribution subject to ASME license or copyright; see http://www.asme.org/terms/Terms_Use.cfm

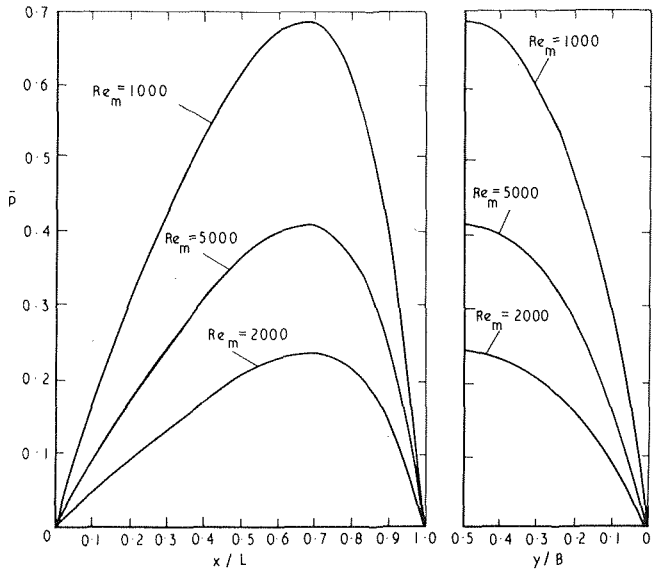

Fig. 10 Dependence of pressure distribution in square pad on Reynolds number; $h_1/h_2 = 2$

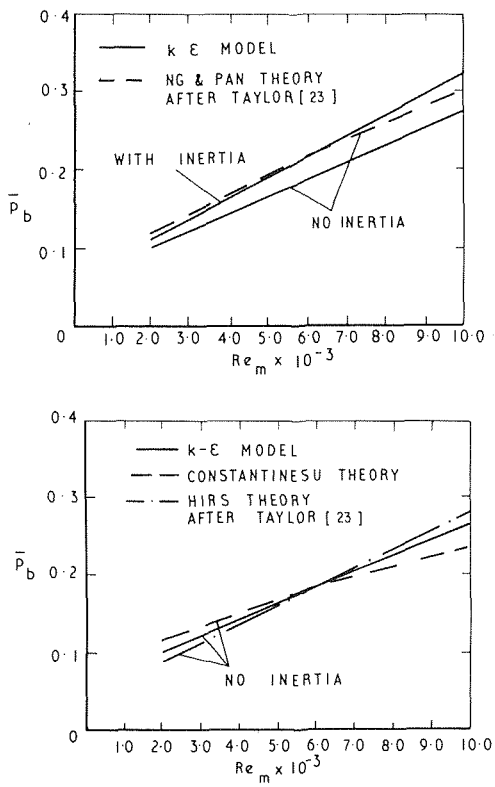

Fig. 11 Variation of load capacity with Reynolds number, a square pad, $h/h_2 = 2$, showing effects of inertia and predictions with other theories

reveals that the k-ϵ model leads to pressure levels significantly below those obtained with Ng and Pan's theory. Better agreement is achieved with the theories of Constantinescu and Hirs. Surprising, in view of the differences shown in Fig. 11(a), is the close agreement that emerges in Fig. 12 between the present solutions for the flow rates and those obtained with Ng and Pan's theory. An explanation for this apparent inconsistency is provided by Fig. 12. This suggests that the nondimensional flow rates are almost independent of the mean pressure (which rises steeply with Re_m). It thus seems that the flow

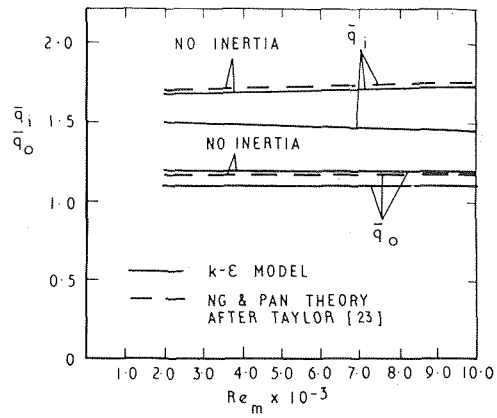

Fig. 12 Variation of normalized flow rates with Reynolds number for square pad, $h_1/h_2 = 2$

rates depend only on the *shape* but not on the magnitude of the pressure field. It may, therefore, be concluded that the shape of the pressure distributions predicted here is very similar to that obtained with Ng and Pan's theory, the only difference lying in the different pressure levels.

Figs. 13 to 16 show the effect of the contraction ratio h_1/h_2 on the pressure, the load capacity, the flow rates and the shear force on the sliding plate. All results relate to a square pad at $\mathrm{Re}_m = 5{,}000$. The film Reynolds number Re* varies between 8 for $h_1/h_2 = 7.5$ and 4.44 for $h_1/h_2 = 3.5$.

As in the case of laminar flows, inertial effects manifest themselves most strongly when the dependence of the operational characteristics on the contraction ratio is examined. In spite of the decreasing film Reynolds number with contraction ratio, inertia is seen to result in a strong increase in mean pressure and frictional force and a corresponding decrease in flow rates (inlet and side leakage flow). A point worthy of particular attention is the shift in the location of maximum mean pressure from $h_1/h_2 = 2.2$ to $h_1/h_2 = 2.6$. Despite the strong effect of inertia, the present inertial mean-pressure solution lies, for a limited range of h_1/h_2, below that obtained for *noninertial* flows with Ng and Pan's theory, as can be seen from Fig. 14(a). As before, much better agreement is achieved with the solution based on Hirs' theory.

7 Conclusions

On the basis of the foregoing study the following conclusions may be drawn:

(i) The turbulent lubrication theory of Ho and Vohr [15], (providing hitherto the most comprehensive turbulence treatment) and the theory of Ng and Pan (7), (which is currently the most popular) appear to overestimate effects of turbulence in lubricating films.

(ii) Effects of inertia may play an important role in determining the optimum configuration of slider bearings.

(iii) It is thought that little scope exists for further improvements in the representation of turbulence and inertial effects within the framework of the integro-differential approach.

Acknowledgments

Support for this research was provided by the Science Research Council through Grant B/RG/5223. The work was undertaken as a part of a collaborative program of research with the Institute of Tribology, Leeds University. We are pleased to acknowledge many helpful exchanges with Dr. C. M. Taylor and Professor D. Dowson of the Institute. Authors' names appear alphabetically.

References

1 Launder, B. E., and Spalding, D. B., *Mathematical Models of Turbulence*, Academic Press, 1972.

2 Constantinescu, V. N., "On Turbulent Lubrication," *Proc. Inst. Mech. Eng.*, England, Vol. 173, 1959, p. 889.

Downloaded 16 Aug 2012 to 165.91.101.108. Redistribution subject to ASME license or copyright; see http://www.asme.org/terms/Terms_Use.cfm

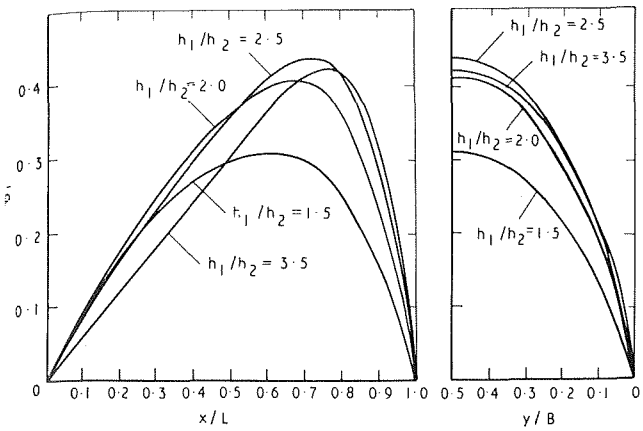

Fig. 13 Effect of contraction ratio on pressure distribution in square pad, $Re_m = 5000$

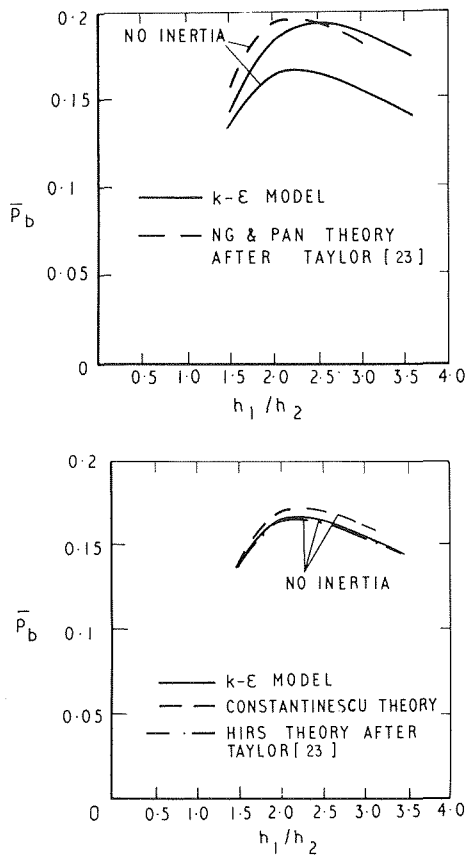

Fig. 14 Variation of load capacity with contraction ratio showing effect of inertia and predictions with other theories; $Re_m = 5000$

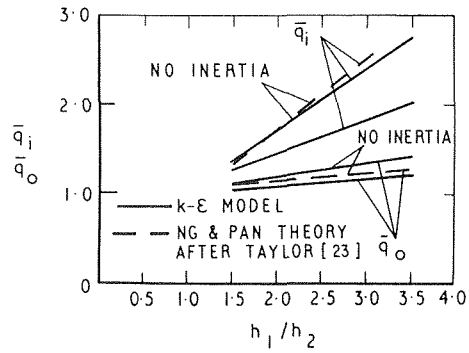

Fig. 15 Variation of normalized flow rates with contraction ratio

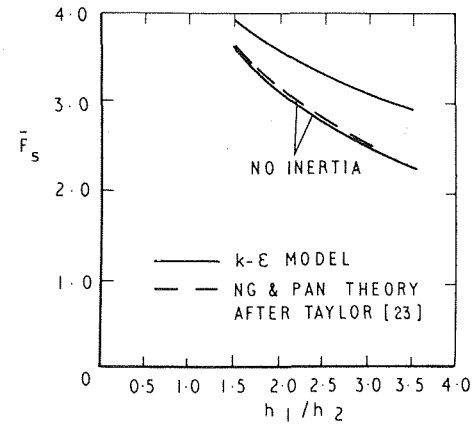

Fig. 16 Normalized shear force on sliding plate as function of contraction ratio

3 Constantinescu, V. N., "Analysis of Bearings Operating in Turbulent Regime," ASME *Journal of Basic Engineering*, Vol. 84, 1962, p. 139.

4 Arwas, E. B., Sternlicht, B., and Wernick, R. J., "Analysis of Plain Cylindrical Journal Bearings in Turbulent Regime," ASME *Journal of Basic Engineering*, Vol. 26, p. 308.

5 Ho, Mein-Kai, and Vohr, J. G., "Application of Energy Model of Turbulence to Calculation of Turbulent Films," ASME JOURNAL OF LUBRICATION TECHNOLOGY, Vol. 96, Special Issue on Turbulence, 1974, p. 95.

6 Reynolds, A. J., "Analysis of Turbulent Bearing Films," *J. Mech. Eng. Sci.*, Vol. 5, 1963, p. 258.

7 Ng, C. W., and Pan, C. H. T., "A Linearized Turbulent Lubrication Theory," ASME *Journal of Basic Engineering*, Vol. 87, 1965, p. 675.

8 Elrod, H. G., Ng, C. W., "A Theory for Turbulent Fluid Films and Its Application to Bearings," ASME JOURNAL OF LUBRICATION TECHNOLOGY, Vol. 89, 1967, p. 346.

9 Hirs, G. G., "A Bulk-Flow Theory for Turbulence in Lubricant Films," ASME Paper No. 72-Lubs-12, (1972).

10 Leschziner, M. A., "Turbulent Flow in Finite Width Bearing Films Including Turbulence Transport and Inertia Effects," PhD thesis, University of London, England, (1976).

11 Jones, W. P., and Launder, B. E., "The Prediction of Laminarization With a Two-Equation Model of Turbulence," *Int. J. Heat and Mass Transfer*, Vol. 15, 1972, p. 301.

12 Jones, W. P., and Launder, B. E., "The Calculation of Low-Reynolds-Number Phenomena With a Two Equation Model of Turbulence," *Int. J. Heat and Mass Transfer*, Vol. 16, 1973, p. 1189.

13 Sharma, B. I., "The Behavior of Swirling Turbulent Boundary Layers Near Walls," PhD thesis, University of London, England, 1975.

14 Sleskin, N. A., and Targ, S. M., "The Generalized Equations of Reynolds," Computes Rendus (Doklady) de L:Academic des Sciences de L'URSS, Vol. 54, 1946, p. 205.

15 Constantinescu, V. N., "On the Influence of Inertia Forces in Turbulent and Laminar Self-Acting Films," ASME JOURNAL OF LUBRICATION TECHNOLOGY, Vol. 92, 1970, p. 473.

16 Launder, B. E., and Leschziner, M. A., "Flow in Finite-Width Thrust Bearings Including Inertial Effects, I-Laminar Flow," ASME JOURNAL OF LUBRICATION TECHNOLOGY, published in this issue pp. 330–338.

17 Daly, B., and Harlow, F. H., "Turbulent Transport Modeling," *Phys. Fluids*, Vol. 13, 1970, p. 2634.

18 Jones, W. P., "Laminarisation in Strongly Accelerated Boundary Layers," PhD thesis, university of London, 1971.

19 Beavers, G. S., Sparrow, E. M., and Lloyd, J. R., "Low Reynolds Number Turbulent Flow in Large Aspect Ratio Rectangular Ducts," ASME *Journal of Basic Engineering*, Vol. 93, 1971, p. 296.

20 Reichardt, H., "Uber die Geschwindigkeitsverteilung in einer gradlinigen turbulenten Couettestromung," *ZAMM* special supplement, S 26, 1956.

21 Robertson, J. M., "On Turbulent Plane-Couette Flow," 6th Midwestern Conference on Fluid Mechanics, University of Austin, Texas, 1959, p. 169.

22 Couette, M., "Etudes sur le frottement des liquides," *Ann. Chem. Phys.*, Vol. 21, 1890, p. 433.

23 Taylor, C. M., and Dowson, D., "Turbulent Lubrication Theory-Application to Design," ASME JOURNAL OF LUBRICATION TECHNOLOGY, Vol. 96, 1974, special issue on Turbulence, p. 36.

Downloaded 16 Aug 2012 to 165.91.101.108. Redistribution subject to ASME license or copyright; see http://www.asme.org/terms/Terms_Use.cfm